Geophys. J. R. astr. Soc. (1980) 63, 23–43

Regional upper mantle *S*-velocity models from phase velocities of great-circle Rayleigh waves

J. J. Lévêque *Laboratoire d'études géophysique des structures profondes, Associé au CNRS No. 195, Institut de Physique du Globe, 4 Place Jussieu, 75230 Paris, Cedex 05, France*

Received 1979 December 21; in original form 1979 May 23

Summary. A linear inversion approach is used to interpret a wide set of great-circle Rayleigh wave phase velocities in terms of regionalized Earth models.

In a first step 'pure-path' fundamental Rayleigh wave phase velocities are estimated by linear regression from great-circle measurements of phase velocity in the period range 150–300 s, using both published and new observations. For these data a method based on the deviations of observed eigenfrequencies from those for a spherically averaged model of the Earth, is used after subtraction of the effect of ellipticity in the range of geometrical optics.

A regionalization of the Earth is fixed *a priori*, models of variation of structure with depth being sought for each region; this regionalization is based on a variation with age, both for oceans and continents. Four regions are distinguished: (1) 'young ocean' regions (age less than 30 Myr), (2) 'old ocean' regions (age greater than 30 Myr), (3) 'shield and platform' regions and (4) 'tectonic' regions.

In a second step, the 'pure-path' phase velocity curves are then interpreted in terms of *S*-wave velocity models by a linear inversion scheme. The resolution of the data with regard to surface structure is discussed, and care has been taken to constrain continental and oceanic crustal structures in the starting models.

In the upper 250 km, the well-known strong difference between oceanic and continental structures clearly appears in the resulting models. In the depth range 300–450 km, no resolvable differences appear between the 'shield and platform' and 'old ocean' models; yet, slight differences between the 'young ocean' and the 'old ocean' models are indicated. Also for the 'tectonic' region, which includes both subduction zones and mountainous areas, the model contains a 2 per cent higher velocity zone between 300 and 450 km depth.

The results are in agreement with independent regional studies and lead to the conclusion that deep lateral *S*-velocity variations are related to recent tectonic processes.

1 Introduction

The existence of deep lateral heterogeneity in the upper mantle has been under question for many years. Very-long-period Rayleigh waves have been used to investigate the *S*-velocity distribution in the upper mantle and its transition region.

A first step is the search for 'pure path' phase velocities. At a given period, the differences between regional velocities are indicative of lateral heterogeneities at depth.

Several regionalizations of the phase velocities observed along great-circles have been performed (Toksöz & Anderson 1966; Kanamori 1970; Dziewonski 1970a). For these first regionalizations, based upon a geological map due to Umbgrove (1949), three regions had been used: oceanic, shield and tectonic-mountainous regions. Kanamori (1970) and Toksöz & Anderson (1966) have shown that the differences between the tectonic and shield regions are larger than the differences between the oceanic and shield regions. For Dziewonski (1970a) on the other hand, only very little phase velocity variations have been found between the three regions. The differences between these first results may probably be explained by the composition of the paths used. Indeed, both of these authors have considered the oceans as an homogeneous region; this assumption seems quite valid for Dziewonski's data, where the average age of the ocean is nearly the same along each great-circle, but is more questionable for Kanamori's data, where the average age of the oceanic path is very different from one great-circle to another (Okal 1977).

Using the concept of plate tectonics, Wu (1972) has regionalized the Earth into four regions (ocean, ridge, continent and arc). The regionalized phase velocities obtained by Wu (1972) from Dziewonski's data (Dziewonski 1970a) show lower velocities for ridge than for oceans between the periods 175 and 300 s. A more detailed regionalization (seven regions) has been proposed by Okal (1977), but the oceanic phase velocities (four regions) have been fixed to the theoretical values predicted by the models of Leeds (1975) (resulting from measurements at shorter periods) which show no lateral variations at depths greater than 120 km. The regionalized phase velocities are computed for the three remaining continental regions: shield, tectonic and mountains. The shield velocities are close to 70 Myr old ocean velocities, and the tectonic velocities are close to the young (15 Myr) ocean velocities. As to Okal (1977), the differences between the average oceanic and the continental velocities are of the same order as the variations within the oceanic plate due to age; the intra-ocean variations may be explained by lateral heterogeneity not deeper than 180 km, and the differences between shield velocities and oceanic ones do not require lateral heterogeneity deeper than 240 km. On the other hand, as to Jordan (1978b), lateral variations inferred from both Love wave dispersion and *ScS* travel time between ocean and continent do persist at depth as great as 400 km, the oceanic velocities being smaller than the continental velocities.

The results of Kanamori have been used in an inversion by Press (1970), and Dziewonski (1971) obtained regional models by inversion of his own results, but oceans had been taken as a whole in the regionalization. In this paper, a regionalization based on age of both oceans and continents takes into account a possible variation of structure with age; then we apply a linear inversion scheme to interpret the regionalized phase velocities in terms of *S*-velocity models. Our results indicate that small lateral heterogeneities probably exist at depths as great as 400 km but, as will be shown, they are not due to a simple continent–ocean difference below 300 km.

2 The data

In addition to the great-circle phase velocities investigated by Kanamori (1970) and Dziewonski (1970a), a new set of great-circle phase velocities has been used in this study

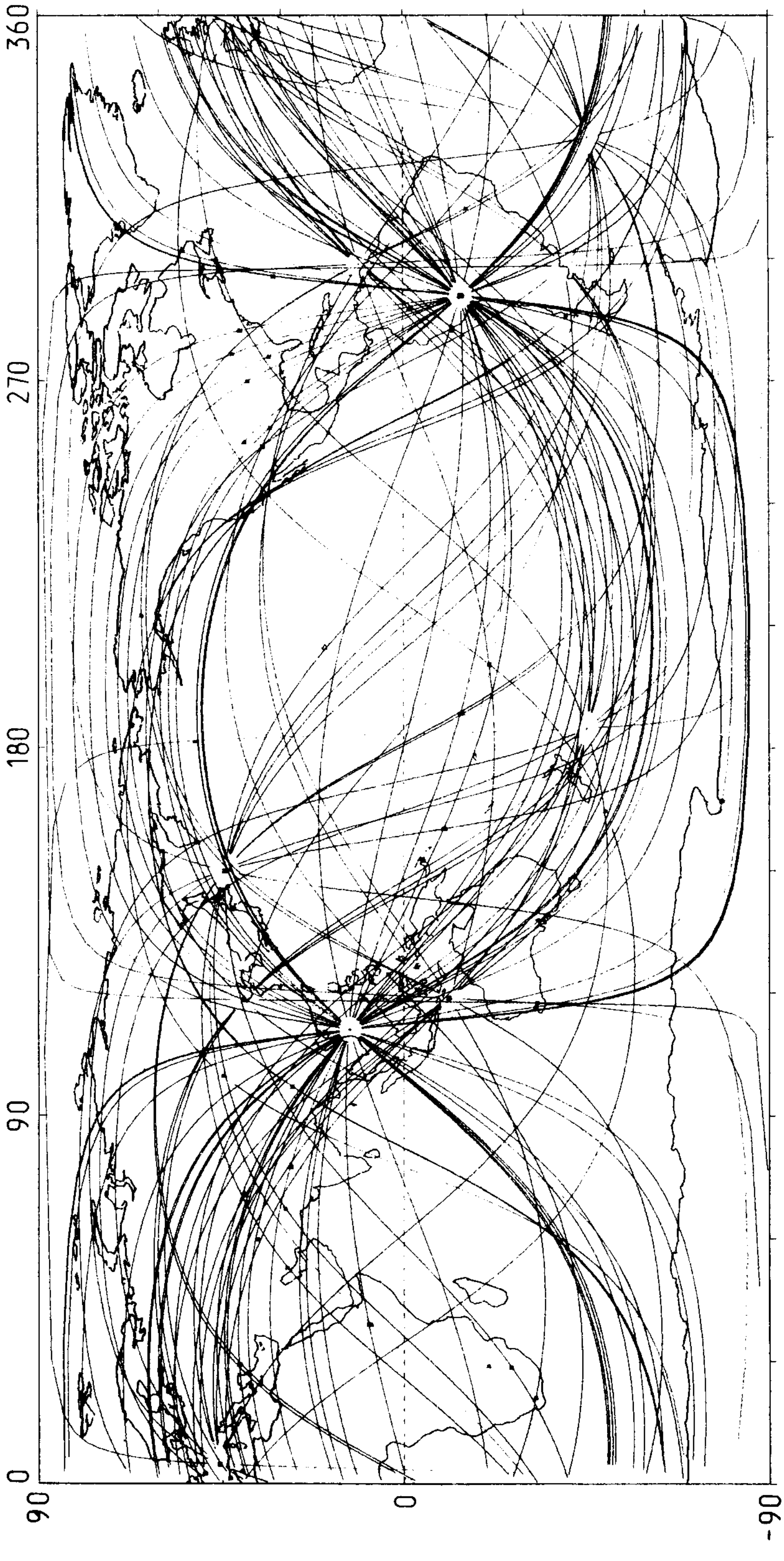

Figure 1. Plot of all the great-circles used in this study.

Table 1. List of paths used and their composition.

1–24: Paths corresponding to free oscillation measurements.
25–33: Paths corresponding to surface wave measurements.
34–91: Paths corresponding to data published by Dziewonski (1970).
92–111: Paths corresponding to data published by Kanamori (1970).

	Event		M_S	Station	path composition			
					young ocean	old ocean	shield platf.	tec-tonic
1	Aleutian Is.	04/02/65	7.5	Strasbourg	0.050	0.516	0.192	0.242
2	Colombia	31/07/70	7.0	I.P.G. *	0.150	0.279	0.196	0.375
3	Celebes Sea	11/06/72	7.5	I.P.G. *	0.142	0.237	0.175	0.446
4	Philippines	02/12/72	7.4	I.P.G. *	0.154	0.212	0.192	0.442
5	Mexico	30/01/73	7.5	I.P.G. *	0.342	0.370	0.071	0.217
6	Kurile Is.	28/02/73	7.2	I.P.G. *	0.146	0.271	0.217	0.366
7	Hokkaido	17/06/73	7.7	I.P.G. *	0.075	0.308	0.250	0.367
8	Peru	03/10/74	7.6	I.P.G. *	0.146	0.267	0.208	0.379
9	China	27/07/76	7.9	ANMO (SRO)	0.142	0.216	0.088	0.554
10	"	"	"	NWAO "	0.083	0.146	0.417	0.354
11	"	"	"	SNZO "	0.067	0.238	0.233	0.462
12	"	"	"	MAIO "	0.167	0.441	0.142	0.250
13	"	"	"	V.Adam (IPG)	0.063	0.246	0.233	0.458
14	"	"	"	Moulis "	0.063	0.233	0.246	0.458
15	Sumba Is.	19/08/77	7.9	CMO (IDA)	0.058	0.258	0.188	0.496
16	"	"	"	BDF "	0.079	0.300	0.175	0.446
17	"	"	"	GAR "	0.221	0.208	0.246	0.325
18	"	"	"	NNA "	0.225	0.196	0.225	0.354
19	"	"	"	HAL "	0.063	0.154	0.375	0.408
20	"	"	"	RAR "	0.221	0.337	0.217	0.225
21	"	"	"	SUR "	0.150	0.517	0.038	0.295
22	"	"	"	V.Adam (IPG)	0.200	0.238	0.254	0.308
23	"	"	"	Moulis "	0.142	0.291	0.192	0.375
24	Philippines	02/12/72	7.4	ALQ (WWSSN)	0.179	0.425	0.125	0.271
25	China	27/07/76	7.9	ANMO (SRO)	0.142	0.216	0.088	0.554
26	"	"	"	NWAO "	0.083	0.146	0.417	0.354
27	"	"	"	SNZO "	0.067	0.238	0.233	0.462
28	"	"	"	MAIO "	0.167	0.441	0.142	0.250
29	"	"	"	V.Adam (IPG)	0.063	0.246	0.233	0.458
30	Sumba Is.	19/08/77	7.9	V.Adam (IPG)	0.200	0.238	0.254	0.308
31	Peru	03/10/74	7.6	St-Sauveur (IPG)	0.146	0.267	0.208	0.379
32	"	"	"	Moulis (IPG)	0.146	0.267	0.208	0.379
33	Mexico	30/01/73	7.5	St-Sauveur (IPG)	0.342	0.370	0.071	0.217
34 35	Peru-Bolivia	15/08/63	8	AAE	0.225	0.371	0.142	0.262
36 37	"	"	"	AAM	0.050	0.146	0.292	0.512
38	"	"	"	ADE	0.188	0.246	0.258	0.308
39	"	"	"	AFI	0.142	0.263	0.287	0.308
40 41	"	"	"	ALQ	0.183	0.204	0.113	0.500
42	"	"	"	ANP	0.292	0.275	0.046	0.387
43 44	"	"	"	AQU	0.125	0.267	0.137	0.471
45 46	"	"	"	ATL	0.046	0.154	0.308	0.492
47 48	"	"	"	ATU	0.121	0.246	0.117	0.516
49	"	"	"	BAG	0.163	0.487	0.100	0.250
50 51	"	"	"	BEC	0.058	0.171	0.338	0.433
52 53	"	"	"	BKS	0.325	0.317	0.042	0.316
54 55	"	"	"	CAR	0.058	0.171	0.338	0.433
56 57	"	"	"	COP	0.229	0.200	0.246	0.325
58 59	"	"	"	FLO	0.042	0.138	0.287	0.533
60 61	"	"	"	GDH	0.058	0.171	0.338	0.433
62 63	"	"	"	GOL	0.092	0.158	0.142	0.608
64 65	"	"	"	GSC	0.325	0.317	0.042	0.316
66	"	"	"	HNR	0.167	0.183	0.279	0.371
67 68	Peru-Bolivia	15/08/63	8	IST	0.117	0.267	0.096	0.520
69	"	"	"	KEV	0.183	0.313	0.171	0.333
70 71	"	"	"	KON	0.237	0.167	0.263	0.333
72 73	"	"	"	LUB	0.125	0.200	0.129	0.546

Table 1 – *continued*

	Event		M_S	Station	path composition: young ocean	old ocean	shield platf.	tec-tonic
74 75	"	"	"	MAL	0.121	0.271	0.133	0.475
76	"	"	"	MUN	0.058	0.183	0.346	0.413
77 78	"	"	"	NDI	0.133	0.221	0.192	0.454
79 80	"	"	"	NUR	0.250	0.158	0.258	0.334
81	"	"	"	RAB	0.167	0.183	0.283	0.367
82	"	"	"	RIV	0.188	0.254	0.250	0.308
83	"	"	"	SBA	0.058	0.254	0.309	0.379
84 85	"	"	"	SCP	0.046	0.171	0.321	0.462
86	"	"	"	SHA	0.038	0.133	0.204	0.625
87	"	"	"	TOL	0.125	0.258	0.171	0.446
88 89	"	"	"	TUC	0.288	0.275	0.046	0.391
90 91	"	"	"	UME	0.154	0.271	0.242	0.333
92 93	Kurile Is.	13/10/63	8.3	AAE	0.238	0.396	0.108	0.258
94	"	"	"	ADE	0.096	0.383	0.217	0.304
95	"	"	"	AFI	0.133	0.483	0.221	0.163
96	"	"	"	BUL	0.221	0.454	0.079	0.246
97	"	"	"	HNR	0.029	0.458	0.058	0.455
98 99	"	"	"	IST	0.133	0.483	0.221	0.163
100	"	"	"	NDI	0.221	0.429	0.083	0.267
101	"	"	"	PRE	0.204	0.471	0.096	0.229
102	"	"	"	QUE	0.234	0.379	0.104	0.283
103	"	"	"	SHI	0.179	0.425	0.167	0.229
104	"	"	"	TOL	0.071	0.288	0.204	0.437
105	Chile	22/05/60	8.3	Pasadena	0.308	0.196	0.013	0.483
106	Alaska	28/03/64	8.5	Isabella	0.383	0.121	0.071	0.425
107	Mongolia	04/12/57	8	Pasadena	0.396	0.100	0.083	0.421
108	Auckland	12/09/64	7.25	Pasadena	0.225	0.375	0.200	0.200
109	Moluccas	24/01/75	7.5	Pasadena	0.146	0.508	0.100	0.246
110 111	Assam	15/08/50	8.5	Pasadena	0.308	0.196	0.013	0.483

* Several records from I.P.G. stations have been used. I.P.G. stations coordinates are:

	Latitude	Longitude
Villier-Adam	49°.07 N	2°.23 E
Moulis	42°.96 N	1°.09 E
Strasbourg	48°.35 N	7°.46 E
St-Sauveur	45°.28 N	4°.54 E

(Table 1, Fig. 1). The phase velocities are derived from the periods of free oscillations observed in a single station by the classic formula: $C=L/T(l+ 05)$ (Jeans 1923), where C is the phase velocity, T the period of the peak at its maximum, l the angular order of the vibration, and L the length of great-circle path between the epicentre and the station. This method has been applied to digital records of the very long period stations of the Institut de Physique du Globe, Paris (IPGP) (Jobert & Roult 1976), Seismic Research Observatories (SRO) stations, and International Deployment of Accelerometers (IDA) stations. A time-variable filtering technique (Cara 1973) applied to the seismograms allows us to isolate the fundamental mode. The eigenperiods measured on this filtered signal are plotted versus the angular order l and a smoothing process is then used before computing the phase velocities (Jobert, Lévêque & Roult 1978).

The theory of geometrical optics used in the regionalization of the phase velocities obtained from eigenvibration spectra fails when the period becomes too large (Madariaga & Aki 1972). We have checked the validity of this method for the periods used in this study by measuring the phase velocities on a single great-circle: the measurement of the phase shift

Table 2. Data processed at the IPGP (differences between the great-circle phase velocities and those listed in Table 3 for model 1066B).

Period (s) no.	150	160	175	200	225	250	275	300	325
1	−0.0060	−0.0029	0.0012	0.0058	0.0076	0.0075	0.0059	0.0034	0.0012
2	–	–	0.0066	0.0053	0.0041	0.0034	0.0031	0.0026	0.0023
3	−0.0052	−0.0025	0.0012	0.0067	0.0102	0.0116	0.0108	0.0085	0.0061
4	0.0001	0.0018	0.0034	0.0049	0.0036	0.0041	0.0049	0.0046	0.0047
5	–	−0.0194	−0.0128	−0.0083	−0.0083	−0.0063	−0.0032	−0.0019	−0.0015
6	0.0060	0.0069	0.0080	0.0087	0.0068	0.0059	0.0047	0.0034	0.0027
7	0.0103	0.0149	0.0153	0.0136	0.0135	0.0126	0.0102	0.0067	0.0035
8	−0.0048	−0.0026	0.0005	0.0052	0.0083	0.0093	0.0083	0.0059	0.0034
9	−0.0129	−0.0115	−0.0081	−0.0007	−0.0001	0.0002	0.0016	0.0028	0.0034
10	0.0103	0.0111	0.0123	0.0109	0.0090	0.0096	0.0120	0.0128	0.0123
11	−0.0050	−0.0018	0.0032	0.0065	0.0034	0.0022	0.0035	–	–
12	0.0005	0.0013	0.0042	0.0063	0.0050	0.0020	−0.0018	–	–
13	0.0001	−0.0001	0.0017	0.0054	0.0035	0.0051	0.0068	0.0086	0.0117
14	−0.0040	−0.0033	−0.0032	−0.0041	−0.0004	0.0049	0.0065	0.0049	0.0026
15	–	–	–	0.0153	0.0145	0.0146	0.0135	0.0121	0.0099
16	–	–	–	–	–	–	–	0.0109	0.0086
17	–	–	0.0030	0.0037	0.0039	0.0038	0.0036	0.0038	0.0042
18	–	–	–	0.0038	0.0014	0.0004	−0.0002	0.0001	0.0006
19	–	–	–	–	0.0210	0.0196	0.0184	0.0151	0.0112
20	–	–	–	0.0029	0.0037	0.0034	0.0046	0.0052	0.0048
21	–	–	–	–	–	–	–	0.0152	0.0145
22	−0.0007	−0.0004	0.0001	0.0009	0.0015	0.0018	0.0017	0.0014	0.0009
23	−0.0013	0.0010	0.0012	0.0017	0.0036	0.0033	0.0024	0.0025	0.0033
24	–	–	–	–	0.0200	0.0129	0.0097	0.0170	0.0176
25	−0.0178	−0.0132	−0.0062	−0.0022	−0.0012	−0.0018	−0.0034	−0.0060	−0.0080
26	0.0132	0.0142	0.0154	0.0096	−0.0038	−0.0072	−0.0078	−0.0062	0.0014
27	−0.0050	−0.0026	0.0018	0.0086	0.0040	0.0020	−0.0028	−0.0050	−0.0062
28	0.0012	0.0030	0.0040	0.0044	−0.0010	−0.0080	−0.0154	−0.0174	−0.0042
29	0.0000	0.0022	0.0054	0.0084	0.0088	0.0048	−0.0002	−0.0046	0.0044
30	0.0000	0.0008	0.0022	0.0044	0.0062	0.0066	0.0036	−0.0050	−0.0100
31	0.0026	0.0050	0.0058	0.0048	0.0030	0.0012	−0.0018	−0.0042	−0.0054
32	0.0004	0.0030	0.0042	0.0042	0.0020	−0.0108	−0.0260	–	–
33	−0.0262	−0.0240	−0.0200	−0.0142	0.0000	0.0072	−0.0010	−0.0092	−0.0088

between two surface wave trains R_i and R_{i+2} recorded at the same station provides phase velocities more closely related to the great-circle path. The results obtained by both methods on a few records are very similar in the period range 150–300 s used in this study, and the two methods are equivalent (Jobert *et al.* 1978). The theoretical proof of this equivalence has been recently given by Dahlen (1979) and Jordan (1978a).

The phase velocities have been obtained mainly from free oscillation spectra, some of them by autocorrelation. The results are given as differences between observed and theoretical phase velocities at the periods used by Kanamori (1970). The global model 1066B (Gilbert & Dziewonski 1975) has been used as reference model in these results (Table 2).

3 Regionalization

As a first approach, the Earth's surface was divided in three regions: young ocean, old ocean, and continents (defined by the 1000 fathoms isobath) (Lévêque 1978). This number of

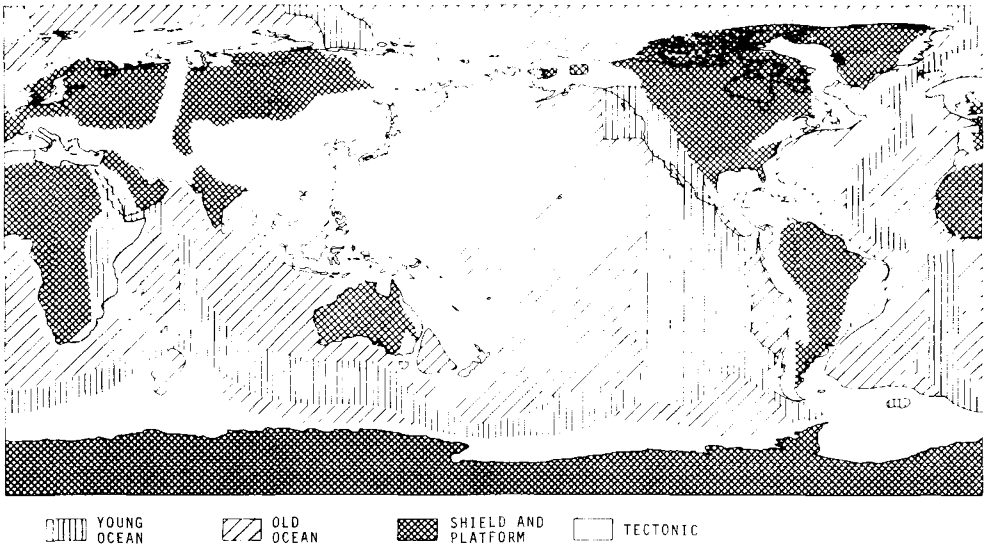

Figure 2. Regionalization of the Earth's surface based upon the age of the sea-floor in the oceans (Pitman *et al.* 1974) and upon tectonic features in continents (Khain & Muratov 1969).

regions is clearly not sufficient (more regions may be distinguished in the continents) but when the number of regions becomes too great, classical instabilities appear in the least squares method. Finally, we have retained the four following regions: 'young ocean', 'old ocean', 'shields and platforms' and a region containing the residual zones, called 'tectonic' (Fig. 2). The 'young ocean'–'old ocean' boundary is defined by the 30 Myr isochron and the 'old ocean' region contains all the oceanic zones older than 30 Myr with the exception of the subduction zones. The ages of the oceanic basins have been drawn from the map of Pitman, Larson & Herron (1974) complemented by a map by Schlich (1975) for the Indian Ocean. The region 'shields and platforms' is drawn from the geological map of Khain & Muratov (1969). The latter region, 'tectonic', is the least homogeneous since it contains both subduction zones and mountains. The path length in each region for each great-circle is listed in Table 1.

'Pure-path' velocities are computed by a least-squares method using the formula:

$$1/C^j = \sum_{i=1}^{4} l_i^j/(L \cdot C_i),$$

Table 3. Differences ΔC between the regionalized phase velocities and those computed for the model 1066B (km s^{-1}); δC, standard deviations for ΔC (km s^{-1}); T, period.

	Young ocean		Old ocean		Shield and platform		Tectonic		
T(s)	ΔC	δC	ΔC	δC	ΔC	δC	ΔC	δC	C_{1066B}
150	−0.0264	0.0107	−0.0011	0.0085	0.0437	0.0093	−0.0167	0.0060	4.3020
160	−0.0366	0.0109	0.0133	0.0072	0.0349	0.0090	−0.0102	0.0055	4.3490
175	−0.0353	0.0064	0.0138	0.0046	0.0272	0.0060	−0.0030	0.0038	4.4262
200	−0.0424	0.0064	0.0204	0.0048	0.0157	0.0060	0.0045	0.0037	4.5714
225	−0.0257	0.0060	0.0170	0.0043	0.0024	0.0054	0.0078	0.0035	4.7351
250	−0.0080	0.0072	0.0084	0.0052	−0.0064	0.0064	0.0105	0.0040	4.9134
275	−0.0192	0.0075	0.0195	0.0055	−0.0084	0.0069	0.0047	0.0043	5.0996
300	−0.0150	0.0082	0.0247	0.0058	−0.0067	0.0074	−0.0009	0.0048	5.2860
325	−0.0414	0.0152	0.0424	0.0096	0.0007	0.0151	−0.0050	0.0104	5.4650

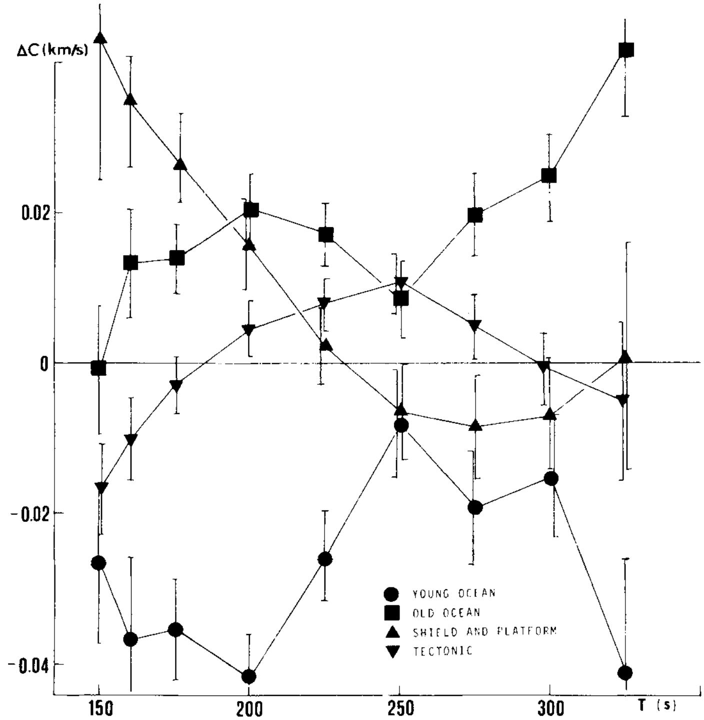

Figure 3. Relative 'pure-path' velocities for the four regions shown in Fig. 2. The zero-line corresponds to the model 1066B (Gilbert & Dziewonski 1975).

where C^j is the measured velocity on the great-circle, l_i^j is the path length in the ith region, L the great-circle length, and C_i the 'pure-path' velocity in the ith region. Resulting phase velocities C_i are listed in Table 3 and plotted on Fig. 3.

4 The ellipticity of the Earth: a check of the method

A good check of the data and of the linear regression approach is to measure a well-known parameter from the great-circle phase velocities: the ellipticity of the Earth, which causes a perturbation on phase velocity about five times smaller than the lateral heterogeneities. In a first step, the average effect of the lateral heterogeneities is supposed to be zero, and no coupling is supposed to exist between the ellipticity of the Earth and the lateral heterogeneities (this assumption is not valid if all the great-circles have a common point, for example if only one epicentre is used; in this case, indeed, both ellipticity and lateral heterogeneities are correlated with the azimuth of the great-circle). The values of e^{-1} found are given versus period in Table 4-A. The average value of e^{-1} is found 265.1 in the period

Table 4. Inverse of the ellipticity e of the Earth, inferred from the great-circle phase velocities by two methods (see the text).

Period	150	160	175	200	225	250	275	300	325
Number of data	33	46	60	74	80	80	75	71	25
e^{-1} (A)	378.7	97.9	174.3	226.1	280.0	433.9	1983.0	−449.7	−34.5
e^{-1} (B)	400.8	124.1	304.3	477.8	343.4	375.6	691.4	−823.2	−32.6

range 150–250 s, rather close to the known value of e^{-1}, 298.3 (Levallois 1969). In a second step, we have searched for both the ellipticity and the lateral variations of phase velocity (Table 4-B). The average value of e^{-1} in the period range 150–250 s is then found 337.7. For periods smaller than 250 s, it is clear from Table 4 that the estimated value of e^{-1} is not far from the actual value. The effect of lateral heterogeneities is much stronger than the ellipticity effect. If the period is not too large, the method may thus provide significant 'pure-path' phase velocities (at least up to 250 s).

5 Discussion of errors

The error bars on regionalized phase velocities have been computed assuming that the error on the phase velocity C^j observed on the jth great-circle does not depend on j and is equal to the average value of the deviations from regression line:

$$\delta C = \left[\sum_j \left| C^j - \frac{1}{L} \sum_i l_i^j \cdot C_i \right|^2 \Big/ \left(\Sigma_i - \Sigma_j \right) \right]^{1/2}.$$

This estimated error arises from two possible origins:

(1) errors in the estimation of the great-circle phase velocities;

(2) error due to the regionalization, if the *a priori* fixed boundaries of the regions are far from the actual boundaries or if the geophysical structure is inhomogeneous inside a region. Two extreme cases are thus possible.

First, if the regionalization was correct, since the least squares method minimizes the deviation δC the error value would be underestimated, unless the great-circle measurement errors were perfectly random around the actual value.

Second, if the measurement errors were negligible, the main part of the error would be caused by an erroneous regionalization. A discussion of this problem has been presented by Knopoff (1972); the 'pure-path' phase velocities would be the average values of the actual velocities in the region, if it is conveniently sampled by the paths, and it would be very reliable although the estimated error is not zero: this error indicates in this case how heterogeneous the region is. In case of a bad sampling, a systematic error could arise. Inspection of Figs 1 and 2 shows that this is not the case for the 'tectonic region'. Lumping together mountains and subduction zones is indeed an over-simplification: if short-period waves were used, a regionalization at a smaller scale should be done, due to the strong variations of crustal thickness for these regions. In this study an effect on long-period waves, almost independent of period, is taken into account. As will be discussed in the next chapter on inversion, the starting models are constrained in the upper 45 km according to the regionalization. A systematic error could arise if the surface structure differs from the actual average structure. For the 'tectonic' regions it is considered that a compensation between thicker and thinner parts of the crust along the numerous great-circle paths through these regions is obtained.

The errors δC given by the above expression for the 'tectonic' region reflect more the heterogeneity of this region than the actual experimental error in estimating the average phase velocity. The measurement error on 'pure-path' phase velocity is, in this case, overestimated.

The computed error bars proceed from a combination of these two effects.

6 Inversion of the data

Searching for the S-velocity model from the 'pure-path' phase velocities is a non-linear inverse problem, but linearization is possible when searching for the perturbation to add to a starting model (Backus & Gilbert 1968). The data of the inversion are then the differences between the observed phase velocities and theoretical phase velocities corresponding to the starting model, and the results of the inversion are perturbations which have to be added to the starting model.

In this way, the 'pure-path' phase velocities found in the four regions have been interpreted in terms of S-velocity models by using the linear inversion scheme of Wiggins (1972). The data used for each inversion are 'pure-path' velocities at the periods 150, 175, 200, 225, 250, 275 and 300 s.

Because of the non-linear dependence between the phase velocity and the model parameters in the crustal layer, the depth range of the inversion has been limited to 45–1405 km (below this latter depth, the influence of the model may be neglected). Only S-velocity has been inverted, P-velocity and ρ (density) being fixed because of their smaller influence.

Indeed, inspection of the partial derivatives of the fundamental Rayleigh wave phase velocities (Wiggins 1968) shows that in the mantle the S-velocity is by far the most influent

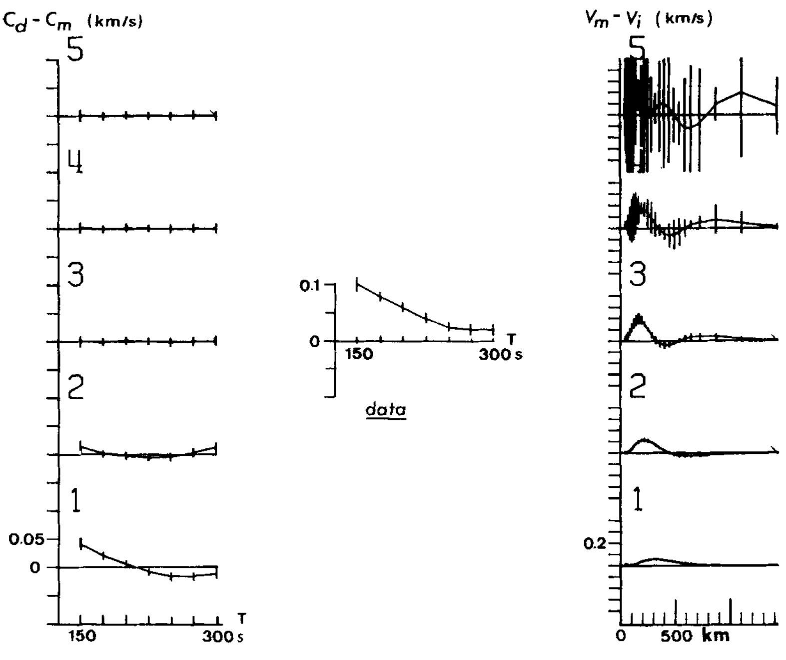

Figure 4. Relative S-velocity models obtained by linear inversion of regionalized phase velocities in the 'shield and platform' region.
Middle: data used in the inversion (differences between the 'pure-path' phase velocities and the starting model phase velocities), versus the period T.
Right: perturbation $V_m - V_i$ to add to the S-velocity V_i of the starting model; $V_m - V_i$ is computed for an increasing number of eigenvectors (decreasing eigenvalues).
Left: differences between the data and the theoretical phase velocities C_m for the corresponding inverted model.
Note that the baseline discrepancy of the data (middle) is taken into account by the one-eigenvector model, the slope by the two-eigenvector model, the curvature by the three-eigenvector model; finally the smaller details and the noise of the data are explained by the models built with more eigenvectors.

parameter, the influence of the *P*-velocity being negligible except in the crust. The importance of density variations comes next to that of the *S*-velocity, but as pointed out by Dziewonski (1970b), with only fundamental mode data it is not possible to isolate unambiguously the effect of density from the effect of *S*-velocity. Thus, in this study, we constrained the density with a model well representative of the average density of the Earth.

6.1 RESOLUTION

Different models have been built with an increasing number of eigenvectors associated with smaller and smaller eigenvalues (Fig. 4). The number of eigenvectors of the final model has been chosen by comparing the fit of the data with the standard deviations of the data. Three eigenvectors is a reasonable choice for all the data sets we have inverted (Fig. 4): nearly all the data are then fitted within their error bars and the error bars of the *S*-velocity models remain generally smaller than 0.04 km s^{-1}. Note also that it is not necessary to change the other parameters, the *P*-velocity or the density, to obtain a good fit of the data. The resolution curves for *S*-velocity are shown in Fig. 5 for a three-eigenvector model. Above a depth of 140 km, the resolution is poor due to the absence of periods smaller than 150 s in the data, and the resulting model has no significance. Below the depth of 800 km, the resolution also becomes poor and no conclusion may be drawn from our data at these depths.

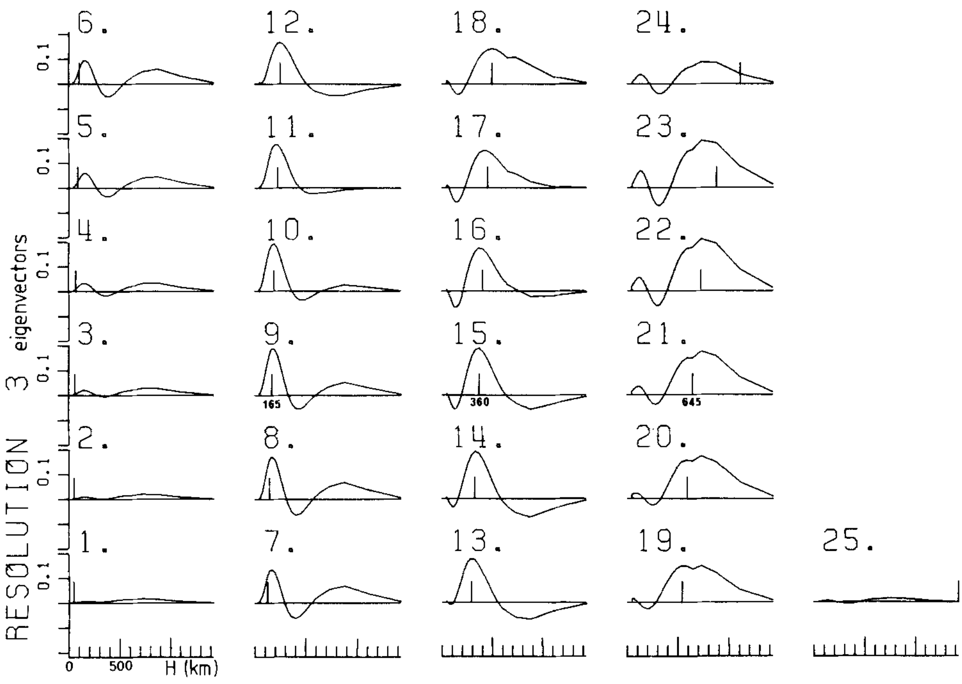

Figure 5. Resolution curves of the three-eigenvector 'shield and platform' model for each of the depths (marked by vertical dash) defined in Table 6 between 45 and 1405 km (see also Fig. 6).

6.2 THE STARTING MODELS

As discussed in the preceding chapter, the starting model has to be very close to the actual average structure in the uppermost 45 km, because of the strong influence of the elastic parameters of the superficial layers on the phase velocity, even for such long periods (150–300 s). The choice of the starting model in the depth range 45–140 km is also important because the resolution is too poor to obtain a significant S-velocity model in this depth range.

For the 'shields and platforms' region, the model 1066A (Gilbert & Dziewonski 1975) has been chosen as a starting model for depths greater than 45 km. A continental crust has been assumed above this depth (see Table 5).

The 'old ocean' starting model is also the model 1066A for depths greater than 45 km. A constant 4.6 km s^{-1} S-velocity in the upper mantle, an oceanic crust as defined by Leeds (1975) for a 100 Myr oceanic model, with a 6 km thick water layer, has been set above 45 km (Table 6).

A 3.8 km thick water layer, a 6.2 km thick crust as defined by Leeds (1975) in his 15 Myr oceanic model has been set in the uppermost part of 'young ocean' starting model;

Table 5. Result of the inversion: H, depth (km); ρ, density (g cm^{-3}); V_P, P-velocity (km s^{-1}); V_S, S-velocity (km s^{-1}); ΔV_S, standard deviation (see text).

Starting model				Resulting models			
				'Shield and platform'		'Tectonic'	
H	ρ	V_P	V_S	V_S	ΔV_S	V_S	ΔV_S
0.00	2.400	4.900	2.800	–	–	–	–
1.00	2.400	4.900	2.800	–	–	–	–
1.00	2.750	6.000	3.470	–	–	–	–
21.00	2.750	6.000	3.470	–	–	–	–
21.00	3.060	6.700	3.790	–	–	–	–
35.00	3.060	6.700	3.790	–	–	–	–
35.00	3.353	8.100	4.600	–	–	–	–
45.00	3.353	7.722	4.583	4.611	0.009	4.584	0.005
51.25	3.355	7.728	4.567	4.594	0.009	4.537	0.006
60.00	3.357	7.737	4.545	4.585	0.014	4.533	0.009
71.25	3.360	7.759	4.519	4.572	0.018	4.496	0.011
85.00	3.365	7.790	4.489	4.572	0.025	4.452	0.016
101.25	3.369	7.837	4.457	4.578	0.034	4.407	0.022
120.00	3.374	7.896	4.422	4.581	0.040	4.363	0.026
141.25	3.380	7.972	4.389	4.577	0.043	4.331	0.028
165.00	3.387	8.055	4.379	4.576	0.040	4.332	0.026
191.25	3.393	8.162	4.387	4.572	0.031	4.362	0.020
220.00	3.405	8.292	4.413	4.565	0.018	4.419	0.012
251.25	3.428	8.430	4.459	4.563	0.009	4.497	0.006
285.00	3.464	8.583	4.530	4.581	0.017	4.596	0.011
321.25	3.514	8.752	4.629	4.634	0.026	4.713	0.017
360.00	3.581	8.935	4.750	4.724	0.028	4.839	0.018
401.25	3.670	9.136	4.886	4.847	0.024	4.968	0.016
445.00	3.752	9.322	5.013	4.978	0.016	5.078	0.010
491.25	3.816	9.480	5.119	5.100	0.008	5.162	0.005
540.00	3.893	9.682	5.249	5.251	0.013	5.269	0.008
591.25	3.990	9.944	5.414	5.435	0.021	5.414	0.013
645.00	4.123	10.296	5.636	5.671	0.025	5.622	0.016
705.00	4.317	10.791	5.952	5.993	0.026	5.930	0.017

Table 6. Result of the inversion: H, depth (km); ρ, density (g cm^{-3}); V_P, P-velocity (km s^{-1}); V_S, S-velocity (km s^{-1}); ΔV_S, standard deviation (see text).

	Starting model			Resulting models			
				Old ocean		Young ocean	
H	ρ	V_P	V_S	V_S	ΔV_S	V_S	ΔV_S
0.00	1.030	1.520	0.000	–	–	–	–
5.70	1.030	1.520	0.000	–	–	–	–
5.70	2.000	1.650	1.000	–	–	–	–
6.00	2.000	1.650	1.000	–	–	–	–
6.00	2.600	5.150	3.000	–	–	–	–
7.40	2.600	5.150	3.000	–	–	–	–
7.40	2.900	6.800	3.900	–	–	–	–
12.10	2.900	6.800	3.900	–	–	–	–
12.10	3.400	8.100	4.600	–	–	–	–
45.00	3.353	7.722	4.583	4.567	0.007	4.551	0.009
51.25	3.355	7.728	4.567	4.552	0.008	4.540	0.010
60.00	3.357	7.737	4.545	4.525	0.011	4.514	0.015
71.25	3.360	7.759	4.519	4.495	0.014	4.488	0.019
85.00	3.365	7.790	4.489	4.453	0.020	4.445	0.028
101.25	3.369	7.837	4.457	4.406	0.027	4.393	0.037
120.00	3.374	7.896	4.422	4.355	0.033	4.333	0.045
141.25	3.380	7.972	4.389	4.310	0.036	4.277	0.048
165.00	3.387	8.055	4.379	4.295	0.033	4.249	0.045
191.25	3.393	8.162	4.387	4.307	0.026	4.250	0.035
220.00	3.405	8.292	4.413	4.345	0.016	4.279	0.020
251.25	3.428	8.430	4.459	4.409	0.007	4.338	0.010
285.00	3.464	8.583	4.530	4.500	0.014	4.429	0.019
321.25	3.514	8.752	4.629	4.617	0.021	4.549	0.029
360.00	3.581	8.935	4.750	4.750	0.023	4.689	0.031
401.25	3.670	9.136	4.886	4.890	0.020	4.838	0.027
445.00	3.752	9.322	5.013	5.015	0.014	4.972	0.018
491.25	3.816	9.480	5.119	5.114	0.007	5.080	0.009
540.00	3.893	9.682	5.249	5.236	0.010	5.210	0.014
591.25	3.990	9.944	5.414	5.394	0.016	5.375	0.023
645.00	4.123	10.296	5.636	5.611	0.020	5.599	0.028
705.00	4.317	10.791	5.952	5.927	0.021	5.919	0.031

at depth between 10 and 120 km, this model is similar to the Forsyth model (1975) for the age 20 Myr. At greater depth, a linear S-velocity variation with depth has been set until 251.7 km, where it reaches smoothly the 1066A model used at greater depth (see Fig. 8).

The starting model for 'tectonic' region is identical to the 'shields and platforms' starting model, the effect of the thick mountain crust and thin oceanic crust being in opposite direction. A more realistic starting model for this region is difficult to define because of the strong variations of the crustal parameters in this region.

6.3 MAIN FEATURES OF THE MODELS

The resulting models are listed in Tables 5 and 6, and are shown in Fig. 6, for each of the four regions.

In the 'shields and platforms' region, no low velocity zone is required by our data: a rather constant 4.5–4.6 km s^{-1} S-velocity is obtained between the Moho and a depth of

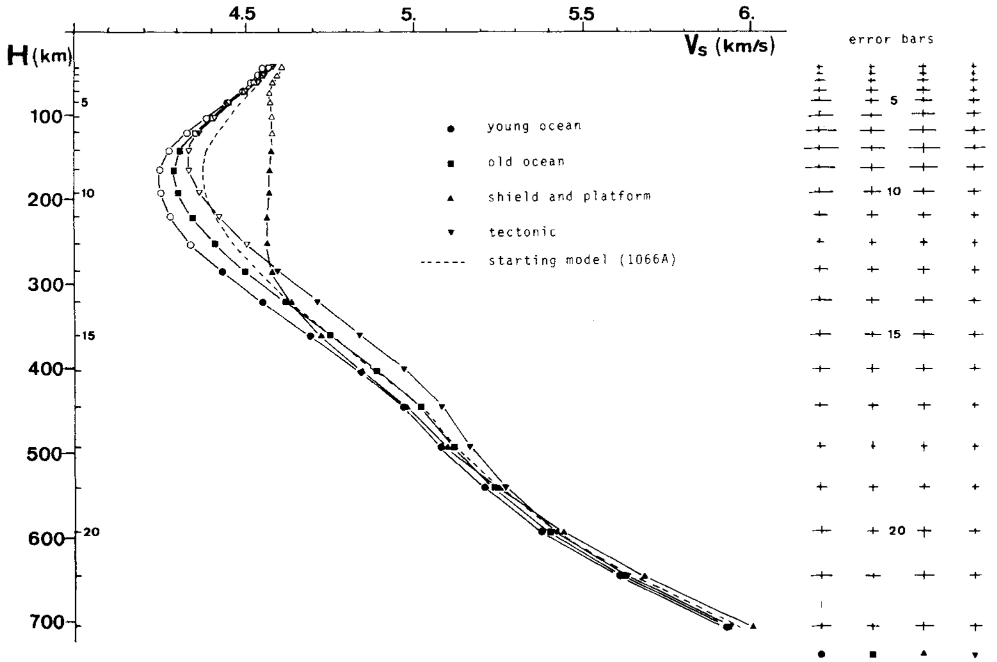

Figure 6. Three-eigenvector S-velocity models obtained from the regionalized phase velocities of Table 3. Empty symbols are used when the confidence is slight. The depths defined in Table 6 are marked on the vertical axis, and the corresponding numbers are the same as in Fig. 5.

about 300 km. Such a feature has been inferred from several regional studies of surface wave dispersion at periods smaller than 150 s (Knopoff 1972; Biswas & Knopoff 1974; Souriau-Thévenard 1976). Note, however, that larger S-velocities in the uppermost part of the mantle are not excluded by our data because of the poor resolution obtained above the depth of 140 km (S_n velocities are often as great as 4.7 km s^{-1} in the platform and shield region; see Huestis, Molnar & Oliver 1973 for example), but an S-velocity value of about 4.57 km s^{-1} constant from 140 km down to 300 km is well established.

The 'tectonic' model exhibits rather low velocities (4.35 km s^{-1}) in the uppermost 300 km, but presents the highest velocities below this depth, down to 500 km. Such a feature of the tectonic model has been put forward by Dziewonski (1971): the tectonic model (T1) is faster than the shield or oceanic model proposed by this author between the depths 200 and 400 km. The excess of S-velocity is of the same order as in our 'tectonic model', but in a homogeneous layer so that the models are not easily comparable. The 'abnormally' large velocities of our tectonic model may be due to the existence of active or non-active subduction zones in the 'tectonic' region defined in Section 3. Note also that it is well-known from body waves that the downgoing slabs are associated with a positive velocity anomaly, both for P- and S-waves (Suyehiro & Sacks 1979).

The 'old ocean' model exhibits much smaller velocities than the shield model in the uppermost 250–300 km of the Earth. The low velocity zone is rather similar to that obtained by Cara (1979) for a 90 Myr lithosphere in the Pacific Ocean, although less pronounced at depths between 80 and 150 km due probably to the lack of resolution of the data used in the present study for this depth range. At greater depths, a remarkable fact is the existence of similar velocities in both 'platforms and shields' and 'old ocean' regions. This result is in agreement with that obtained by Cara (1978), Cara, Nercessian & Nolet (1980) from higher mode data when comparing 'Northern Eurasia' with the 'Pacific Ocean'.

The 'young ocean' region exhibits slightly lower velocities than the 'old ocean' region down to 500 km. This difference is only 0.06 km s^{-1} at 300 km, slightly greater than the standard deviation and its validity is discussed in the next section. Another question discussed in the Appendix, is the influence of the starting model on the above inferences, mainly for the depth range where the resolution is poor.

The above general features of the different models show that, in a first approximation, no strong lateral variations of *S*-velocity are found below the depth of 300 km, except perhaps in the tectonic zones. Unlike the conclusions made by Jordan (1978b), no systematic ocean–continent variations seem to exist at depths as great as 400 km. On the other hand, the conclusion made by Okal (1977) that no lateral variations exist below the depth of 240 km is not in agreement with our data: our data requires lateral heterogeneities deeper than 300 km but they are not a simple continent–ocean variation; for example, lateral variations seem to exist within the 'ocean' regions down to 500 km.

7 Conclusion

'Pure-path' Rayleigh wave phase velocities have been computed from great-circle measurements, after correction for ellipticity.

The data used in this study are in part already published: mainly those of Dziewonski (1970a and b) and Kanamori (1970). To these data we add our own results for several earthquakes, derived from spectra on long-period records (French stations, SRO and IDA stations). For our data, the residuals of great-circle phase velocities have been obtained (Jobert *et al.* 1978) from deviations of the measured eigenfrequencies from those of the global model 1066A (Gilbert & Dziewonski 1975); indeed these deviations have been shown theoretically (Jordan 1978; Dahlen 1979) to reflect an average of ellipticity and lateral heterogeneity effects along the great-circle path through epicentre and station.

The regionalization used here has been determined according to the age of oceans and continents. Before application of linear regression analysis to this regionalization, the resolving power of the data and the method have been successfully checked for their ability to extract the effect of ellipticity, which is about five times smaller than that of the lateral heterogeneities under study.

Fig. 7 shows the results of a linear inversion of the estimated 'pure-path' velocities: *S*-velocity models relative to the global model 1066A of Gilbert & Dziewonski (1975). The surface features of the models have been constrained down to 45 km, using respectively continental and oceanic models of the crust. The effect of a surface change on the deeper part of the models has been checked: they are very stable for depths larger than 300 km.

The *S*-velocity contrast between ocean and continent in the upper 250 km of the Earth has been inferred from these data, and no evidence – at least deeper than 140 km – is found for the existence of a low-velocity zone under the 'shield and platform' region.

The deepest part of the regional *S*-velocity models, obtained by linear inversion, exhibits the following features:

(1) in the 'tectonic' region, an approximately 2 per cent higher velocity is found in the depth range 300–500 km;

(2) the 'young ocean' region shows about 1 per cent smaller velocities than the 'old ocean' region down to 500 km, although the differences are at the limit of the error bars of the models;

(3) no lateral variation between 'old ocean' and 'shield and platform' regions are resolved deeper than 300 km.

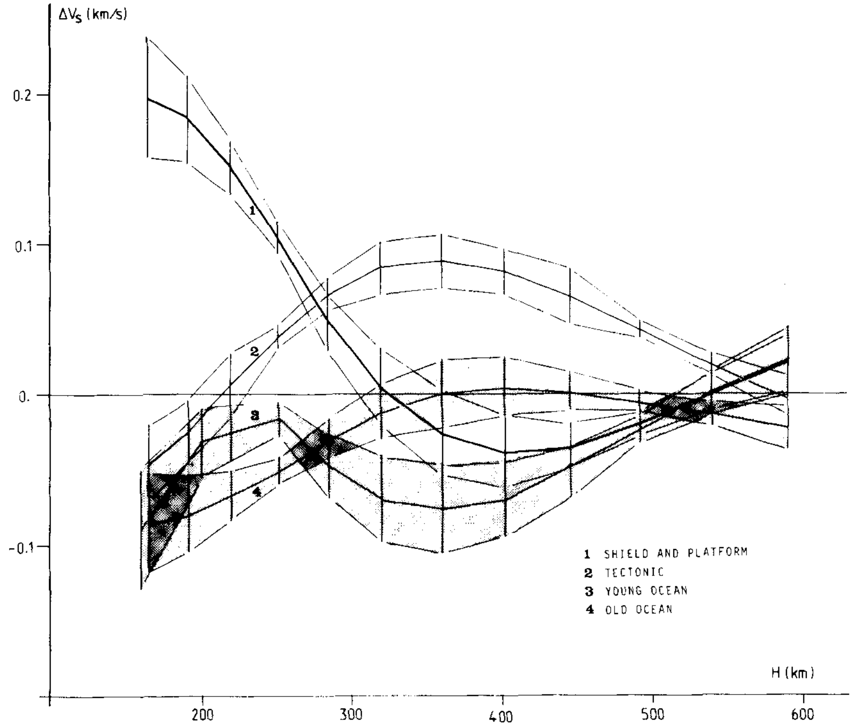

Figure 7. Relative *S*-velocity models in the four regions (the model 1066A is chosen as zero line): 'shield and platform' model (1); 'tectonic' model (2); 'old ocean' model (3); 'young ocean' model (4), inverted by using the starting model 1 plotted in Fig. 7.

The above results have been obtained assuming fixed vertical boundaries between the different regions. If, at a given depth, these boundaries differ from the actual boundaries, in the deeper part of the models for example, the variations obtained in this study are smaller than the true ones (Knopoff 1972). An inversion of the data with no *a priori* fixed boundaries at great depths, out of the scope of the present study, could lead to greater lateral heterogeneities.

In conclusion, unlike Jordan (1978b), from these results no lateral variations deeper than 300 km appear between old oceans and continents. This has been proposed by Okal (1977), assuming oceanic models with lateral variations no deeper than 180 km, by comparison of their velocities with the derived continental velocities. We find here a similar result between old oceans and continents, comparing the models obtained by inversion of entirely regionalized velocities. Yet we find lateral heterogeneities (*S*-velocity differences of the order of 0.1 km s^{-1}) at depths between 300 and 500 km; they are restricted to young regions: 'tectonic', (including subduction zones) with a positive variation, and 'young oceans' with a negative one, suggesting a correlation between these deep anomalies and recent tectonic processes.

Acknowledgments

I thank Nelly Jobert who suggested and directed this research, Michel Cara for many helpful discussions, and F. Dahlen for his suggestions. I am grateful to Geneviève Roult who participated to the processing of the data.

This is contribution I.P.G. No. 365.

References

Backus, G. & Gilbert, F., 1968. The resolving power of gross Earth data, *Geophys. J. R. astr. Soc.*, **16**, 169–205.

Biswas, N. N. & Knopoff, L., 1974. The structure of the upper Mantle under the United States from the dispersion of Rayleigh waves, *Geophys. J. R. astr. Soc.*, **36**, 515–539.

Cara, M., 1973. Filtering of dispersed wave trains, *Geophys. J. R. astr. Soc.*, **33**, 65–80.

Cara, M., 1978. Etude du Manteau supérieur à partir des harmoniques des ondes de surface, *Thèse de Doctorat d'Etat*, Université Paris VI, Paris.

Cara, M., 1979. Lateral variations of *S*-velocity in the upper Mantle from higher Rayleigh modes, *Geophys. J. R. astr. Soc.*, **57**, 649–670.

Cara, M., Nercessian, A. & Nolet, G., 1980. New inferences from higher Rayleigh modes in Western Europe and Northern Eurasia, *Geophys. J. R. astr. Soc.*, **61**, 459–478.

Dahlen, F. A., 1979. The spectra of unresolved multiplets, *Geophys. J. R. astr. Soc.*, **58**, 1–34.

Dziewonski, A. M., 1970a. On regional differences in dispersion of Mantle Rayleigh waves, *Geophys. J. R. astr. Soc.*, **22**, 289–325.

Dziewonski, A. M., 1970b. Correlation properties of free-period partial derivatives and their relation to the resolution of gross Earth data, *Bull. seism. Soc. Am.*, **60**, 741–768.

Dziewonski, A. M., 1971. Upper Mantle models from 'pure-path' dispersion data, *J. geophys. Res.*, **76**, 2587–2601.

Forsyth, D. W., 1975. The early structural evolution and anisotropy of the oceanic upper Mantle, *Geophys. J. R. astr. Soc.*, **43**, 103–162.

Gilbert, F. & Dziewonski, A. M., 1975. An application of normal mode theory to the retrieval of structural parameters and source mechanisms from seismic spectra, *Phil. Trans. R. Soc. Lond.*, **278**, 187–269.

Huestis, S., Molnar, P. & Oliver, J., 1973. Regional S_n velocities in the upper Mantle, *Bull. seism. Soc. Am.*, **63**, 469–475.

Jeans, J. H., 1923. The propagation of earthquake waves, *Proc. R. Soc. Lond. A*, **102**, 554–574.

Jobert, N. & Roult, G., 1976. Periods and damping of free oscillations observed in France after sixteen earthquakes, *Geophys. J. R. astr. Soc.*, **45**, 155–176.

Jobert, N., Lévêque, J. J. & Roult, G., 1978. Evidence of lateral variations from free oscillations and surface waves, *Geophys. Res. Lett.*, **5**, 569–572.

Jordan, T. H., 1978a. A procedure for estimating lateral variations from low frequency eigenspectra data, *Geophys. J. R. astr. Soc.*, **52**, 441–455.

Jordan, T. H., 1978b. Composition and development of the continental tectosphere, *Nature*, **274**, 544–548.

Kanamori, H., 1970. Velocity and *Q* of mantle waves, *Phys. Earth planet. Interiors*, **2**, 259–275.

Khain, V. E. & Muratov, M. V., 1969. Crustal movements and tectonic structure of continents, The Earth's crust and upper Mantle, *Geophys. monogr. 13*, 523–538, ed. Hart, P. J., *Am. geophys. Un.*, Washington D.C.

Knopoff, L., 1972. Observation and inversion of surface wave dispersion, the upper Mantle, *Tectonophysics*, **13**, 497–519.

Leeds, A. R., Knopoff, L. & Kausel, E. G., 1974. Variations of upper Mantle structure under the Pacific Ocean, *Science*, **186**, 141–143.

Leeds, A. R., 1975. Lithospheric thickness in the Western Pacific, *Phys. Earth planet. Interiors*, **11**, 61–64.

Levallois, J. J., 1969. *Géodésie Générale*, tome 2, p. 99, Collection scientifique de l'I.G.N., éd. Eyrolles, Paris.

Lévêque, J. J., 1978. Régionalisation du Manteau supérieur à l'aide des ondes de surface de très longues périodes, *Thèse de 3ème cycle* Université Paris XI.

Madariaga, R. & Aki, K., 1972. Spectral splitting of toroidal free oscillations due to lateral heterogeneity of the Earth's structure, *J. geophys. Res.*, **77**, 4421–4431.

Nakanishi, I., 1978. Regional differences in the phase velocity and quality factor *Q* of Mantle Rayleigh waves, *Science*, **200**, 1379–1381.

Okal, E. A., 1977. The effect of intrinsic oceanic upper Mantle heterogeneity on regionalization of long period Rayleigh wave phase velocities, *Geophys. J. R. astr. Soc.*, **49**, 357–370.

Pitman, W. C., Larson, P. L. & Herron, E. M., 1974. *The Ages of the Oceans Basin (map)*, Geological Society of America.

Press, F., 1970. Regionalized Earth models, *J. geophys. Res.*, **75**, 6575–6581.

Schlich, R., 1975. Campagne océanographique dans l'océan Indien, *Courrier du C.N.R.S. No. 17*, Juillet 75, 14–23.

Souriau-Thévenard, A., 1976. Structure of the crust and upper Mantle in the South-West of France from surface waves, *Ann. Géophys.*, **32**, 63–69.

Suyehiro, K. & Sacks, I. S., 1979. *P*- and *S*-wave velocity anomalies associated with the subducting lithosphere determined from travel time residuals in the Japan region, *Bull. seism. Soc. Am.*, **69**, 97–114.

Toksöz, M. N. & Anderson, D. L., 1966. Phase velocities of long period surface waves and structure of the upper Mantle, *J. geophys. Res.*, **71**, 1649–1658.

Umbgrove, J. H. F., 1949. *The Pulse of the Earth*, 2nd edn, Nijhoff, The Hague.

Wiggins, R. A., 1972. The general inverse problem: implication of surface waves and free oscillations for Earth structure, *Rev. Geophys. Space Phys.*, **10**, 251–285.

Wiggins, R. A., 1968. Terrestrial variational tables for the periods and attenuation of the free oscillations, *Phys. Earth planet. Interiors*, **1**, 201–266.

Wu, F. T., 1972. Mantle Rayleigh wave dispersion and tectonic provinces, *J. geophys. Res.*, **77**, 6445–6453.

Appendix: influence of the starting model

To check the dependence between the starting model and the final model, the 'pure-path' phase velocities for the 'young ocean' region have been inverted by using three different starting models (Fig. 8). These models differ only in the upper 250 km. See Section 6.1 for the first starting model; the second 'young ocean' starting model is identical to that used in the 'old ocean' region. The third starting model is similar to the 15 Myr oceanic model of Leeds (1975) in the upper 45 km, and to the model 1066A (Gilbert & Dziewonski 1975) at depths greater than 165 km; between 45 and 165 km, a linear *S*-velocity variation has been set.

The results of the inversions corresponding to the three starting models are given in Fig. 9. Between 300 and 500 km, the resulting models are rather insensitive to the starting model. The regular and symmetric shape of the resolution curves in this depth range are responsible for this insensitivity to the starting model and the results of the inversion may be generally considered as reliable between 300 and 500 km. Below 500 km, the results depend upon the starting model, due to the shape of the resolution curves (see Fig. 5), but the differences remain small as compared to the standard errors of the models (Fig. 7).

For depths above 300 km, the shape of the resulting models are correlated with the starting models. The results are thus not significant if the starting model is far from the actual structure. The reason for this correlation seems rather clear: because of a poor resolution in depth, the calculated three-eigenvector model is the result of adding a smooth perturbation to a starting model. If fine details are present in the starting model, they still remain in the resulting model; these fine details are not significant, but the average perturbation on a depth range of about 100 km is significant. For example, the resulting model for the 'young ocean' region is smooth when the starting model is smooth, and presents discontinuities if the starting model presents discontinuities (Fig. 8). On the other hand, the differences between (1) the 'shields and platforms' model and (2) the average 'young ocean' or 'old ocean' models, are significant above the depth of 300 km.

In Section 6.2, the 'tectonic' phase velocities have been inverted by using a continental starting model. As it is difficult to define a more realistic model for the region (subduction zones in oceanic domain are mixed up with mountainous zones), an attempt has been made

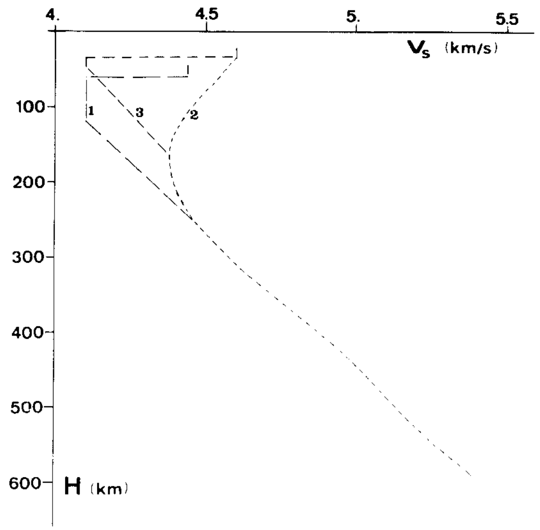

Figure 8. Starting models used for the 'young ocean' region.

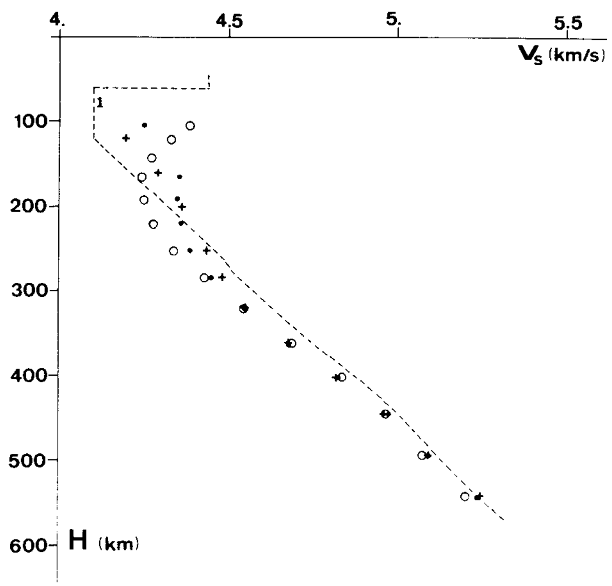

Figure 9. Resulting *S*-velocity models for the 'young ocean' region, obtained by using the different starting models shown in Fig. 7: crosses for model 1 (shown on the figure), circles for model 2, and dots for model 3.

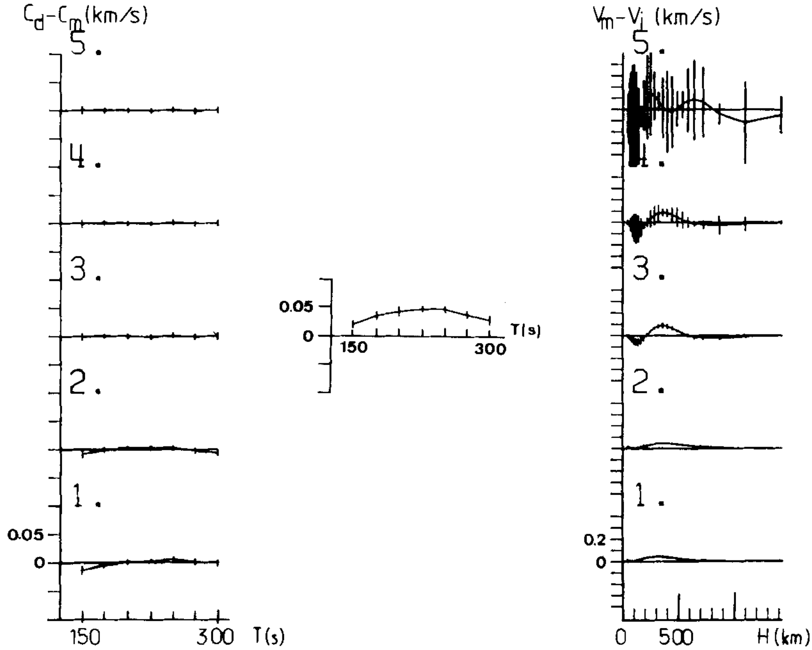

Figure 10. Inversion of the 'tectonic' region data. See caption for Fig. 4.

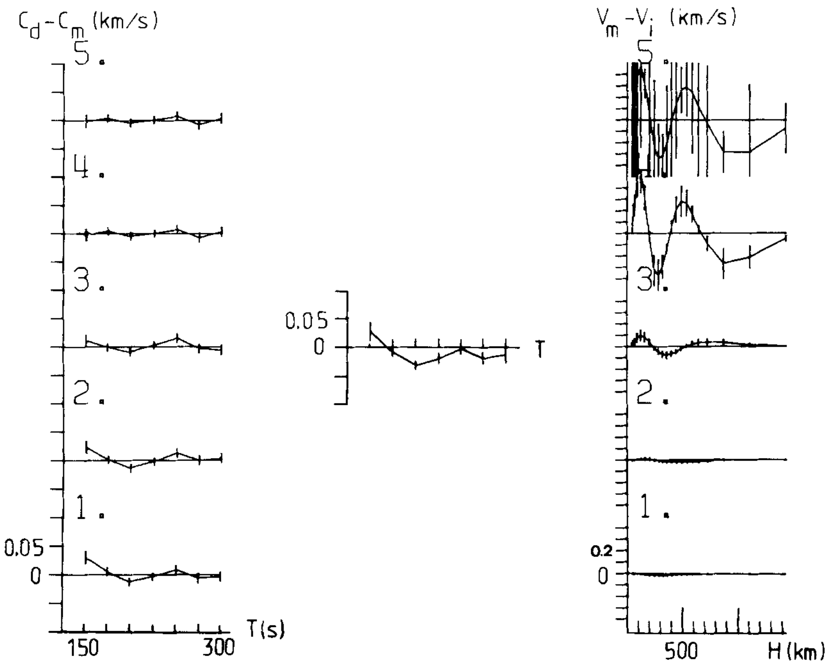

Figure 11. Inversion of the 'young ocean' region data by using the starting model 1 shown in Fig. 7. See caption for Fig. 4.

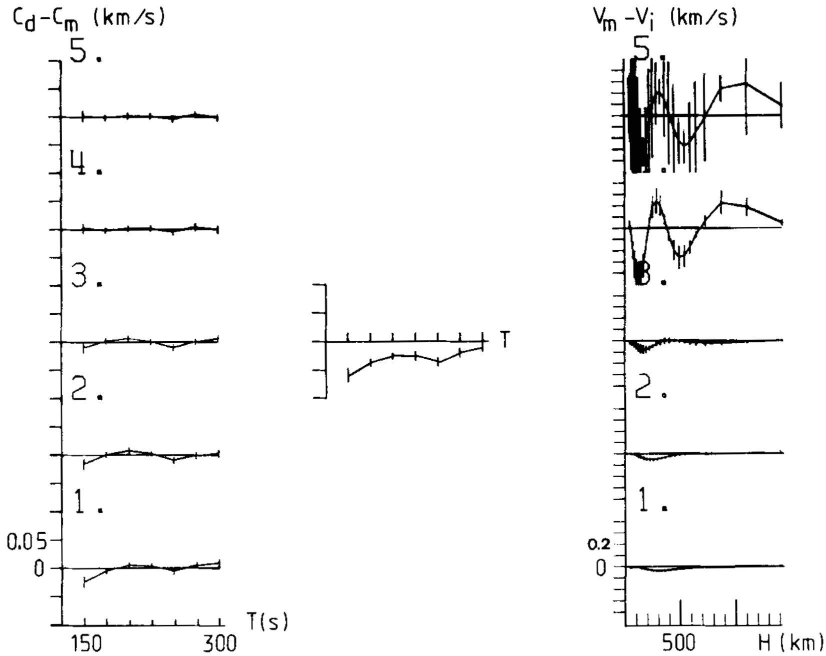

Figure 12. Inversion of the 'old ocean' region data. See caption for Fig. 4.

to inverse the 'tectonic' data with an extremely different starting model: the 'old ocean' starting model, that presents too high velocities between the depths 12 and 45 km for this region. Although they are less pronounced, it is remarkable that the abnormally high velocities in the depth range 300–450 km are still present after this second inversion. These high velocities seem thus well established in the 'tectonic' region.